

# Fluid dynamic behavior of dispensing small droplets through a thin liquid film

Minh Do-Quang · Laurent Geyl · Göran Stemme ·  
Wouter van der Wijngaart · Gustav Amberg

Received: 4 August 2009 / Accepted: 26 November 2009 / Published online: 22 December 2009  
© Springer-Verlag 2009

**Abstract** This paper presents a technology for dispensing droplets through thin liquid layers. The system consists of a free liquid film, which is suspended in a frame and positioned in front of a piezoelectric printhead. A droplet, generated by the printhead, merges with the film, but due to its momentum, passes through and forms a droplet that separates on the other side and continues its flight. The technology allows the dispensing, mixing and ejecting of picolitre liquid samples in a single step. This paper overviews the concept, potential applications, experiments, results and a numerical model. The experimental work includes studying the flight of ink droplets, which ejected from an inkjet print head, fly through a free ink film, suspended in a frame and positioned in front of the printhead. We experimentally observed that the minimum velocity required for the 80 pl droplets to fly through the  $75 \pm 24 \mu\text{m}$  thick ink film was of  $6.6 \text{ m s}^{-1}$ . We also present a numerical simulation of the passage of liquid droplets through a liquid film. The numerical results for different initial speeds of droplets and their shapes are taken into account. We observed that during the droplet–film interaction, the surface energy is partially converted to kinetic energy, and this, together with the impact time, helps the droplets penetrate the film. The model includes the Navier–Stokes equations with continuum-surface-tension force

derived from the phase-field/Cahn–Hilliard equation. This system allows us to simulate the motion of a free surface in the presence of surface tension during merging, mixing and ejection of droplets. The influence of dispensing conditions was studied and it was found that the residual velocity of droplets after their passage through the thin liquid film well matches the measured velocity from the experiment.

**Keywords** Droplet · Dispensing · Fluid dynamic · Simulation

## 1 Introduction

Technologies and methods for small liquid droplet handling and dispensing are used in many applications today, including inkjet printing in the publishing market (Le 1998), and microarray spotting (Barbulovic-Nad et al. 2006). Dispensing of biological liquids in small volume, including proteins, DNA and even whole cells, is of increasing importance in life sciences. Many devices and techniques have been developed for that purpose, e.g. Ducrée et al. (2000) and Jianping and Guiling (2004).

The use of droplet dispensing technology for biotechnical applications is common, however, not uncomplicated due to demands on compatibility between the ejector operation (heat, electric field, pneumatic pressure, etc.) and the liquid properties of sample (biological nature, fouling, viscosity, conductivity, saturation pressure, etc.). Moreover, the dead volume of a dispenser may require more liquid sample for priming the device than is physically available or than is economically viable in life science applications.

In this work we suggest a general approach for allowing the commercially available low-cost dispensers

M. Do-Quang (✉) · G. Amberg  
Linné Flow Centre, Department of Mechanics, The Royal  
Institute of Technology (KTH), 100 44 Stockholm, Sweden  
e-mail: minh@mech.kth.se

L. Geyl · G. Stemme · W. van der Wijngaart  
Microsystem Technology, School of Electrical Engineering,  
The Royal Institute of Technology (KTH), 100 44 Stockholm,  
Sweden

used in the inkjet publishing industry to be used for the dispensing of liquid samples of interest in the field of life sciences. We accomplish this by decoupling the dispensing actuation from the liquid to be dispensed.

## 2 Device description

The dispensing technology in this paper was first introduced by Geyl et al. (2006) and allows for ejecting picolitre amount of liquid from a very small initial sample volume. The system consists of a droplet dispenser and one or more free liquid film(s) suspended in a frame in front of the dispenser, much like a soap film in a soap bubble frame (Fig. 1). Droplets ejected by the dispenser fly through the liquid film(s). The ejected droplets and the film liquid mix partially while the droplets pass through, thus the initial “dispenser droplet” forms a transport medium for the liquid in the free liquid film. When the resulting “film droplet” is captured on a target plate, it can be used for further analysis.

This approach has a number of distinct benefits:

- The liquid suspension frame can be fabricated as a passive and low-cost component, allowing this part of the device to be disposable.
- The liquid film can have a very small volume, thus avoiding large dead volumes.
- We can make use of commercially available low-cost dispensing systems to eject the dispenser droplet.
- The sample volume is not in contact with any other liquids prior to dispensing, thus reducing the risk for sample dilution or contamination.

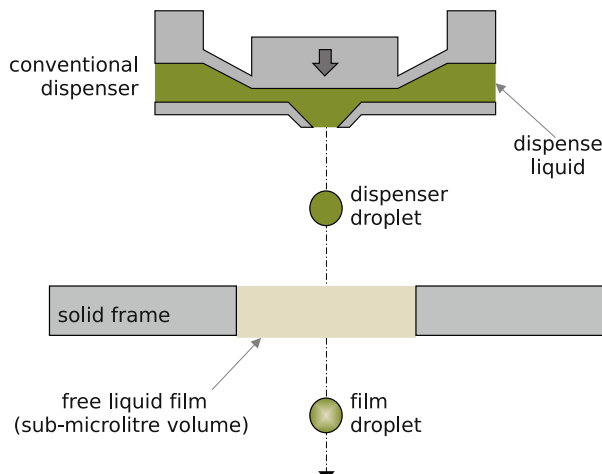


**Fig. 1** Cross-sectional schematic of the new method for sample transport. A dispenser droplet flies through a freestanding liquid film, suspended in a frame, and transports part of the film liquid with it

Forming a free liquid film on the macroscale typically requires low surface tension liquid (cf. soap bubbles). On the microscale, the liquid frame is relatively thick in comparison with the span of the free liquid film, making the formation of microscale free liquid films uncomplicated. The liquid in the dispenser can typically be a buffer solution, which is available in larger quantities at low cost. The liquid volume required to form the free liquid film is typically much smaller than the dead volume of a dispenser. This method thus suits applications where the amount of available sample is limited.

The minimum initial sample volume required equals the amount necessary to form the free liquid film. Another benefit of the novel approach is that the buffer liquid in the dispenser can be tailored for reliable dispensing characteristics. For example, dispense liquids should not foul the internal dispenser surface and have appropriate surface tension characteristics. Only few dispense liquids are required to serve as transport medium for a multitude of sample liquids. Thus, this novel approach eases adapting available printhead systems for dispensing of a large range of liquids of interest in life sciences.

The novel method forms further a general approach to transport picolitre sample volume from a microfluidic (lab-on-chip) environment to another carrier, for example for further analysis. For this purpose, the microfluidic system must be modified with an interfacing window to allow the flight of dispenser droplets through the system, as illustrated in Fig. 2. Parallelising this scheme renders a versatile system for producing microarrays, as illustrated in Fig. 3. In the illustrated system, the dispenser droplet flies through two free liquid films before being captured on a target plate.

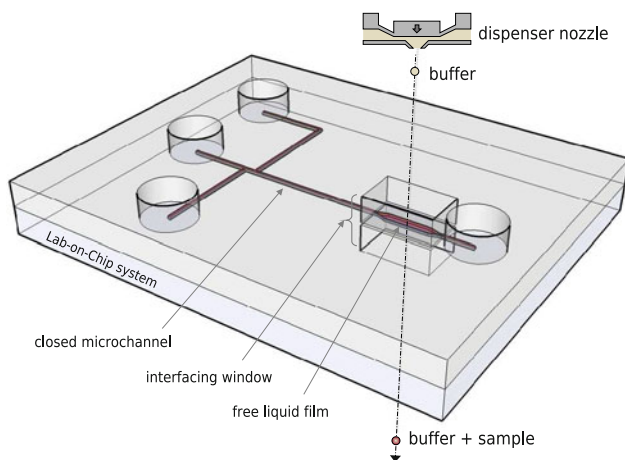
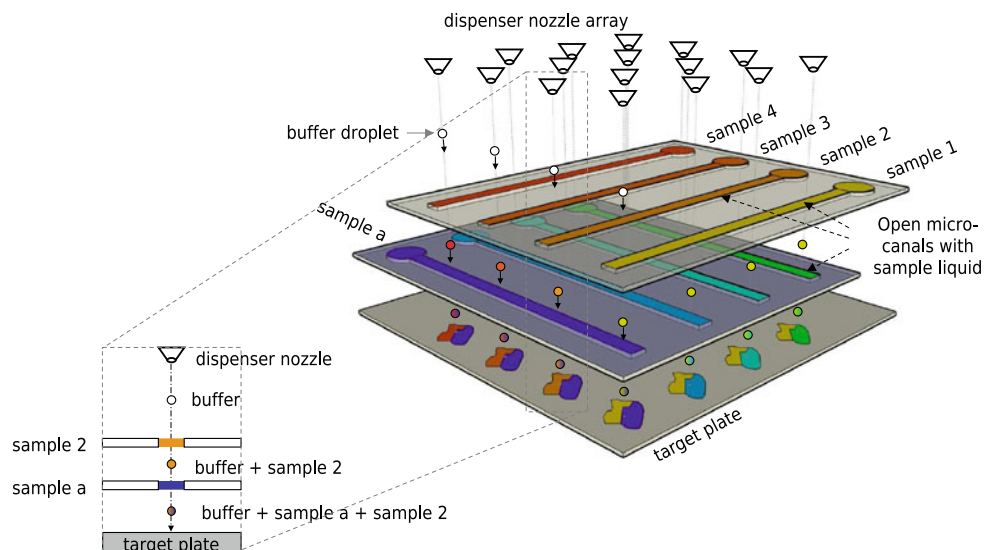


**Fig. 2** Conceptual view of a lab-on-chip system adapted with an interfacing window to enable sample extraction using the novel method

**Fig. 3** Conceptual view on a system for generating microarrays of sample mixtures. Each nozzle in the array fires droplets of buffer liquid through two liquid films (open microchannels without “floor” and “ceiling”) placed in the path of the droplet. Each liquid film contains sample liquid, which partially mixes with the passing buffer droplet. After passing the two liquid films, the droplet thus consists of a mixture of buffer and both samples. Capturing these droplets on a target plate forms an array of unique sample mixtures



### 3 Experimental setup

Our experimental work investigated the flight of small liquid droplets through a thin liquid film. For this purpose, we adapted the standard printhead test equipment of the printhead manufacturer Xaar. The setup consists of a rectangular glass frame positioned in front of a commercial piezoelectric inkjet printhead (Xaar XJ128). The glass frame formed a  $1.25 \times 1.75 \text{ mm}^2$  square window for suspending a free liquid film. The measurement setup further incorporated a stroboscopic camera for visualisation and measurement of droplet velocity and volume. The piezoelectric XJ128 printhead can only handle non-conductive liquids with an appropriate surface tension. We therefore chose oily ink as liquid during this proof-of-concept investigation. This had the additional benefit that the evaporation rate was limited, making the formation of stable suspended liquid films easier. The printhead was filled with transparent ink; the free suspended liquid film consisted of black ink. Both the black and the transparent inks have a viscosity  $\mu = 0.01 \text{ N s m}^{-2}$ , a density  $\rho = 880 \text{ kg m}^{-3}$  and a surface tension  $\gamma = 0.032 \text{ N m}^{-1}$ .

First we measured the thickness of the black ink film suspended in the glass frame using the needle contact method. The ink film was positioned vertically and two needles, one on each side of the liquid surface and facing each other, were moved horizontally towards the film using a micropositioner. When a needle touches the liquid interface, a change in surface curvature is easily detected with the naked eye. After both needles were moved until they were both in contact with the liquid, one of the needles was moved further until it reached the other needle. The needle–needle contact was detected via an electrical resistance measurement. In this setup, a precision of 5  $\mu\text{m}$

could be reached with the micropositioner. In 49 independent measurements the liquid film thickness  $h$  varied between 39 and 121  $\mu\text{m}$ , with an average estimated thickness  $h = 75 \pm 24 \mu\text{m}$  (Fig. 4).

Thereafter we studied the flight of dispenser droplets through a liquid film. For this purpose, we fired droplets at a fixed frequency of 50 Hz. The dispenser droplet velocity,  $u_1$ , was varied between 4 and 11  $\text{m s}^{-1}$  by varying the dispensing power of the printhead. A stroboscopic measurement setup was used to measure the droplet velocity (Fig. 5).

#### 3.1 Experimental results and discussion

No measurable change in radius, and thus volume, of the dispenser droplets was observed with varying operation voltage. The dispenser droplet radius and volume were  $R_1 \approx 27 \mu\text{m}$ , and  $V_1 \approx 80 \text{ pl}$ , respectively. The dispenser

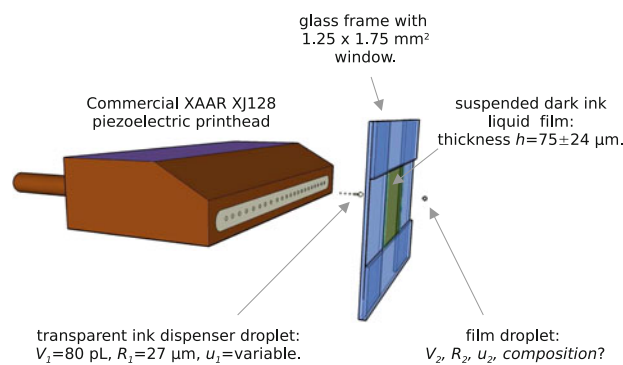
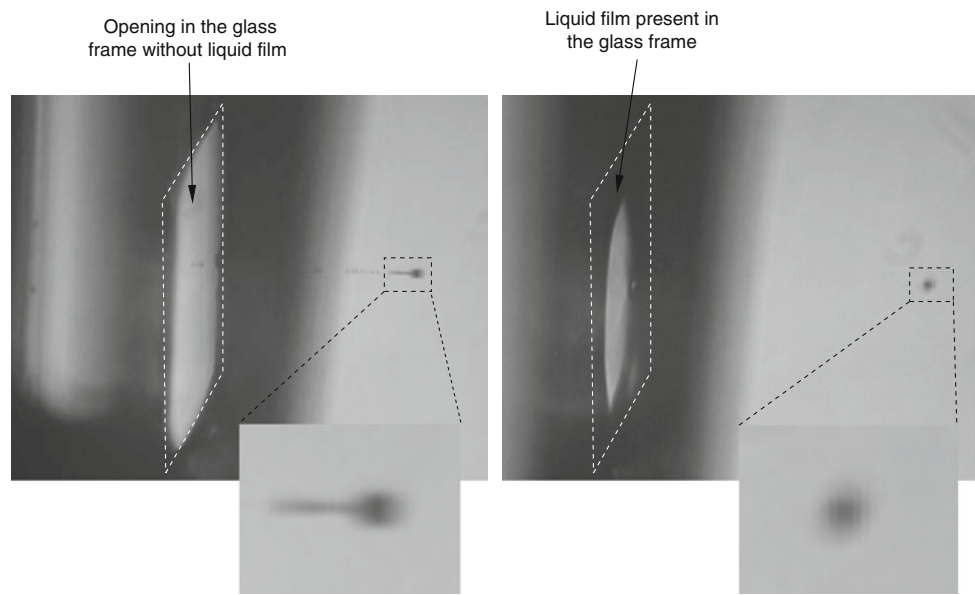


**Fig. 4** Schematic of the experimental setup used to study the flight of a dispenser droplet through a suspended free liquid film

**Fig. 5** Microscope pictures of a dispenser droplet with satellites, ejected prior to filling the frame with a liquid film (*left*), and a film droplet, i.e. after passing through a free liquid film, under the same dispensing conditions (*right*)



droplet velocity,  $u_1$ , was varied between 4 and 11 m s<sup>-1</sup>. When the dispensing velocity,  $u_1$ , was below a critical velocity  $u^* = 6.6$  m s<sup>-1</sup>, the droplet merges with the free liquid film upon impact. When  $u_1 > u^*$ , the droplet flies through the liquid film and a film droplet appears on the other side, with velocity  $u_2$ . One can observe that the printhead ejected droplets feature satellites. However, after flying through the liquid film, no satellites remain. The system thus functions as a filter for satellite droplets. A change in the film droplet radius,  $R_2$ , compared to the dispenser droplet radius,  $R_1$ , was not observed. However, the film droplet velocity,  $u_2$ , was strongly dependent on the dispensing droplet velocity,  $u_1$ , as shown in Fig. 6.

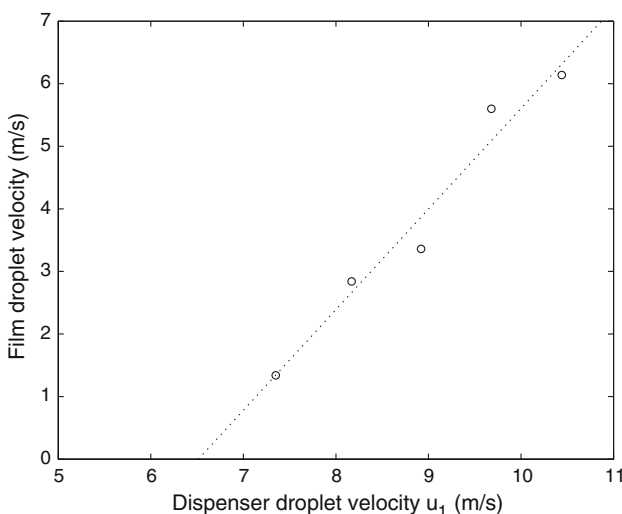


**Fig. 6** The measured film droplet velocity  $u_2$  plotted versus the dispensing velocity  $u_1$ . Linear regression shows the critical velocity  $u^* \approx 6.6$  m s<sup>-1</sup> required to generate film droplets

#### 4 Analytical model

A simplified analytical model assumes the droplet as a solid sphere moving through a fluid, with a flow profile similar to that of steady Stokes flow around a spherical object. The Reynolds number for a velocity  $u_1 \approx 10$  m s<sup>-1</sup> and droplet diameter  $2R_1 \approx 54$  μm is  $Re \approx 53$ , i.e. the system is in the laminar regime. The boundary layer thickness around the sphere  $\delta \propto \sqrt{\frac{\mu}{\rho} \cdot \frac{R}{u_1}} \approx 5.2$  μm  $< R_1$  indicates that modelling the droplet as a solid sphere is not unreasonable. The system can be described using the laws of energy conservation, taking into consideration the kinetic energy,  $E_k = \frac{m \cdot u^2}{2}$ , and the surface tension energy,  $E_s = 4\pi R^2 \gamma$ , of both the dispensed droplet (index 1) and film droplet (index 2):

$$E_{k,1} + E_{s,1} = E_{\text{loss}} + E_{k,2} + E_{s,2}. \quad (1)$$

The term  $E_{\text{loss}}$  includes the energy losses occurring when the droplet moves through the liquid film. The surface tension energy terms are equal ( $R_1 \approx R_2 = R$ ) and much smaller than the kinetic energy of the dispenser droplet, and they can thus be neglected. The total energy loss of the droplet through viscous losses can be expressed using Stokes equation for drag:

$$F_{\text{drag}} = -6\pi\mu Ru(x) = m \frac{du(x)}{dt}, \quad (2)$$

with  $m = \frac{4}{3}\pi R^3 \rho$  the droplet mass. The use of Eq. 2 could be questionable here, since it is strictly valid only when the Reynolds number is less than unity. However, in the present Reynolds number range,  $1 < Re < 50$ , Eq. 2 still captures the dependency of fluid drag on velocity better than the corresponding high Reynolds number formula. The droplet position,  $x$ , and velocity  $u(x) = \frac{dx}{dt}$  can thus be expressed as

$$x(t) = \frac{m}{6\pi\mu R} u_1 \left[ 1 - \exp\left(-\frac{6\pi\mu R}{m} t\right) \right], \text{ and} \quad (3)$$

$$u(t) = u_1 \exp\left(-\frac{6\pi\mu R}{m} t\right) = u_1 - \frac{6\pi\mu R}{m} x(t). \quad (4)$$

For a film droplet to appear after moving through the complete film thickness  $h$ , the condition

$$u|_{x=h} = u_1 - \frac{6\pi\mu R}{m} h = u_1 - \frac{6\pi\mu R}{\frac{4}{3}\pi R^3 \rho} h > 0 \quad (5)$$

must be fulfilled. Thus, the theoretical critical velocity  $u^* = \frac{9}{2} \frac{\mu h}{\rho R^2} = 5.26 \text{ m s}^{-1}$ , which apparently is in accordance with the experimentally obtained value of  $6.6 \text{ m s}^{-1}$ .  $E_{\text{loss}}$  can now be expressed as

$$E_{\text{loss}} = 6\pi\mu R \int_0^h u(x) dx = 6\pi\mu Rh \cdot [u_1 - u^*]. \quad (6)$$

In Fig. 7, both the theoretical and the measured kinetic energy of the film droplet are plotted versus the dispensing velocity. A good match between measurement and theory can again be observed.

## 5 Numerical modelling

To obtain a better understanding of the experimentally observed fluidic behaviour, a numerical model was constructed.

### 5.1 Governing equations

In our phase-field model, the order parameter, a phase-field  $\phi$ , is assumed to have a distinct constant value in each

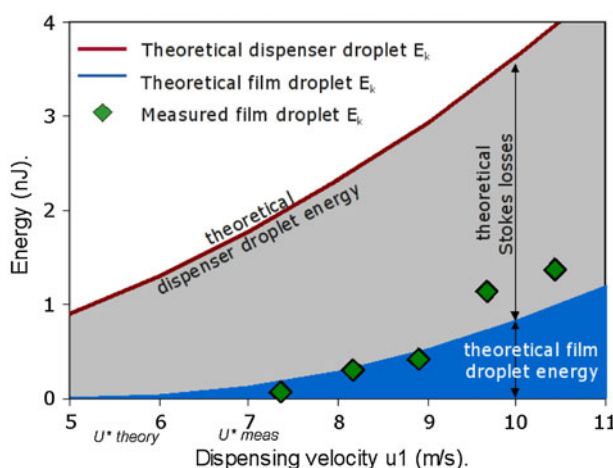


**Fig. 7** The theoretical and measured kinetic energy of the dispenser droplets and the film droplets versus the dispensing velocity

phase and to change rapidly but smoothly in the interface region. For example,  $\phi = 1$  in liquid phase and  $\phi = -1$  in gas phase. The free energy of the system often referred to as a Ginzburg-Landau expansion,

$$\mathcal{F} = \int_{\Omega} \left( \beta\psi(\phi) - \frac{1}{2}\alpha\nabla^2\phi \right) d\Omega, \quad (7)$$

where  $\alpha$  and  $\beta$  are constants that are related to the surface tension and interface thickness.  $\psi(\phi)$  represents the bulk energy of a homogeneous phase, describing the regions far from the interface, see Cahn and Hilliard (1958). In our model,  $\psi$  is a double-well potential function that has two minima at  $\phi = \pm 1$  corresponding to the two stable phases. A simple example of such a function is,

$$\psi = (\phi + 1)^2(\phi - 1)^2. \quad (8)$$

The second term in Eq. 7 describes the interface energy. This term associates with variations of the phase field  $\phi$  and contributes the free energy of the interfacial region, which defines the surface tension coefficient, Villanueva and Amberg (2006),

$$\sigma = \alpha \int_{-\infty}^{+\infty} \left( \frac{d\phi_0}{dx} \right)^2 dx = \frac{2\sqrt{2}}{3} \sqrt{\alpha\beta} \quad (9)$$

The fluid flow is described by the Navier-Stokes equations for an incompressible axisymmetric two-phase flow.

$$\frac{\partial \rho \mathbf{u}}{\partial t} + \mathbf{u} \cdot (\nabla \rho \mathbf{u}) = -\nabla p + \nabla \cdot [\mu(\nabla \mathbf{u} + (\nabla \mathbf{u})^T)] - \eta \nabla \phi, \quad (10)$$

$$\nabla \cdot \mathbf{u} = 0, \quad (11)$$

$$\frac{\partial \phi}{\partial t} + (\mathbf{u} \cdot \nabla) \phi = \nabla \cdot (\kappa \nabla \eta), \quad (12)$$

where  $\rho$  denotes the density,  $\mathbf{u}$  the velocity vector,  $\mu$  the viscosity and  $p$  the pressure. The last term in Eq. 10 represents the surface tension which is related to the phase-field variables, Jacqmin (1999).

The interface is captured by using the phase-field method (Jacqmin 1999; Villanueva and Amberg 2006), which replaces a sharp interface by a finite thickness, smooth transition region. The phase field  $\phi$  is governed by the convective Cahn–Hilliard equation, Eq. 12. Here,  $\kappa$  is the constant mobility and  $\eta$  is the chemical potential, defined as

$$\eta = \beta \frac{\partial \psi}{\partial \phi} - \alpha \nabla^2 \phi. \quad (13)$$

Once the phase field is calculated, the physical properties such as the density and the viscosity are calculated as follows,

$$\rho = \rho_l \frac{1 + \phi}{2} + \rho_g \frac{1 - \phi}{2}, \quad (14)$$

$$\mu = \mu_l \frac{1 + \phi}{2} + \mu_g \frac{1 - \phi}{2} \quad (15)$$

where  $\rho_l$ ,  $\rho_g$  and  $\mu_l$ ,  $\mu_g$  are the densities and viscosities of the liquid and gas phase, respectively.

## 5.2 Boundary conditions

Neumann conditions are described for the inlet and outlet boundary. The slip boundary condition with zero shear stress for the side and the symmetry edges (Fig. 8). Two boundary conditions are needed for the Cahn–Hilliard equation,

$$\mathbf{n} \cdot \nabla \phi = 0, \quad (16)$$

where  $\mathbf{n}$  is the unit vector normal to the wall, and,

$$\mathbf{n} \cdot \nabla \eta = 0. \quad (17)$$

## 5.3 Non-dimensionalisation

Define the dimensionless variables,

$$x' = \frac{x}{L_c}, u' = \frac{u}{U_c}, t' = \frac{tU_c}{L_c}, p' = \frac{p}{\rho_c U_c^2}, \quad (18)$$

where  $L_c$  is the characteristic length taken to be the thickness of the thin film,  $U_c$  is the characteristic velocity

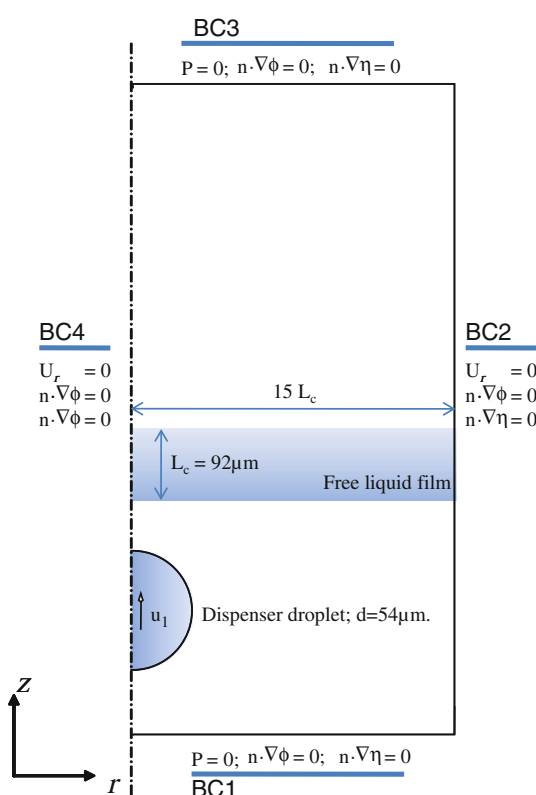


**Fig. 8** Boundary conditions

taken to be the critical velocity in the experiment,  $U_c = 6.6 \text{ m s}^{-1}$ .  $\rho_c$  is the characteristic density defined as the water density. Dropping the primes, the dimensionless equations are

$$\frac{D(\rho(\phi)\mathbf{u})}{Dt} = -\nabla p + \frac{1}{Re} \nabla \cdot [\mu(\phi)(\nabla \mathbf{u} + (\nabla \mathbf{u})^T)] - \frac{1}{Ca \cdot Cn \cdot Re} \eta \nabla \phi, \quad (19)$$

$$\nabla \cdot \mathbf{u} = 0, \quad (20)$$

$$\frac{D\phi}{Dt} = \frac{1}{Pe} \nabla \cdot (\kappa \nabla \eta), \quad (21)$$

$$\eta = \frac{\partial \psi}{\partial \phi} - Cn^2 \nabla^2 \phi. \quad (22)$$

Note that incompressibility does not imply that the density is constant, only that the density is independent of pressure, which is a good approximation whenever flow speeds are small compared to speeds of sound. Also, note that the Peclet number in Eq. 21 is large, due to the small value of the diffusion coefficient. Equation 21 then essentially states that  $\phi$ , and thus density, is constant along a streamline, which is consistent with the assumption of incompressibility in Eq. 20.

The dimensionless parameters are the Capillary number  $Ca$ , Reynolds number  $Re$ , Peclet number  $Pe$  and Cahn number  $Cn$ ,

$$Ca = \frac{\mu_c U_c}{\sigma}, Re = \frac{\rho_c U_c L_c}{\mu}, Pe = \frac{U_c L_c}{D}, Cn = \frac{\xi}{L_c}, \quad (23)$$

where  $\mu_c$  is the characteristic viscosity taken to be the water viscosity,  $D$  is the difusivity of liquid vapour in air,  $\xi = \sqrt{\alpha/\beta}$  is the interface thickness.

## 6 Numerical treatment

The numerical simulations were carried out using femLego (Amberg et al. 1999), a symbolic tool to solve partial differential equations with adaptive finite element methods. The partial differential equations, boundary condition, initial conditions and the method of solving each equation are all specified in a Maple worksheet. The Cahn–Hilliard equation is treated as a coupled system for the chemical potential  $\eta$  and the composition  $\phi$ . Both chemical potential and composition equations are discretised in space using piecewise linear functions and discretised in time using an implicit scheme. The coupled linear systems of  $\eta$  and  $\phi$  are solved simultaneously using the unsymmetric multifrontal method (UMFPACK), Davis (2004).

To ensure mesh resolution along the vicinity of the interface, an adaptively refined and derefined mesh is used with an ad hoc error criterion function,

$$\epsilon \int_{\Omega_k} \nabla^2 C \leq \text{tol.} \quad (24)$$

The implementation of the mesh adaptivity can be described as follows. At each mesh refinement step, an element  $\Omega_k$  is marked for refinement if the element size is still larger than the minimum mesh size allowed,  $h > h_{\min}$ , and it does not meet the error criterion (24).  $\epsilon$  is an ad hoc parameter. In the case that an element meets the error criterion, it is marked for derefinement unless it is an original element. At the next refinement step, elements containing hanging nodes are marked for refinement. The refinement/derefinement stops if and only if no element is marked for refinement/derefinement. More details about this scheme can be found in Do-Quang and Amberg (2009), Do-Quang et al. (2007) and Villanueva and Amberg (2006).

The Navier–Stokes equations are solved using a projection method for variable density that was introduced by Guermond and Quartapelle (2000). The Navier–Stokes equations are also discretised in space using piecewise linear functions with the convective term treated as a semi-implicit term which allows a longer time step in the computations. The linear system is solved by the generalised minimal residual method (GMRES).

## 7 Numerical results and discussion

We begin with the illustration of the behaviour of a droplet, which impacts and passes through to be a free hanging liquid thin film, by consideration of a small, non-evaporating droplet having the diameter of  $2R = 54 \mu\text{m}$ . The droplet is moving toward the thin liquid film,  $L_c = 92 \mu\text{m}$  thick, at a given initial speed. Both the droplet

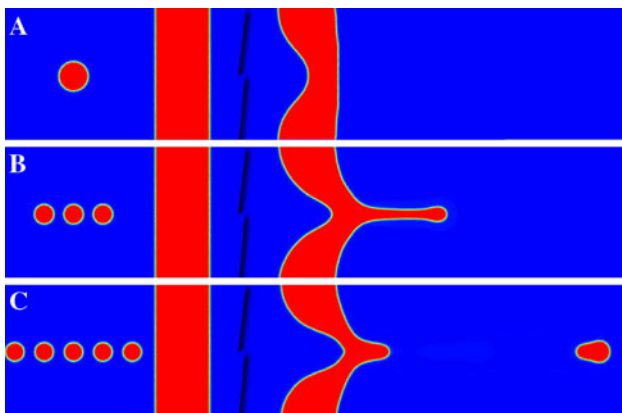


**Fig. 9** The solution at  $t = 0$  (left) and  $t = 45.6 \mu\text{s}$  (right) for three different initial conditions

and the thin film have the same material properties: density of  $\rho = 880 \text{ kg m}^{-3}$ , viscosity of  $\mu = 0.01 \text{ N s m}^{-2}$  and surface tension of  $\sigma = 0.032 \text{ N m}^{-1}$ . The computational domain chosen is a cylindrical region,  $6L_c$  in radius and  $15L_c$  long.

In accordance with the experiment, we tried to shoot a single droplet at a thin liquid film at different speeds from  $u_1 = 6$  to  $13.2 \text{ m s}^{-1}$ . No second droplet created in the other side of the film had been observed in all tested speeds as seen in the experiment. All droplets were trapped in the film. The left panel in Fig. 9a shows the initial condition for a case with a single droplet at the initial speed

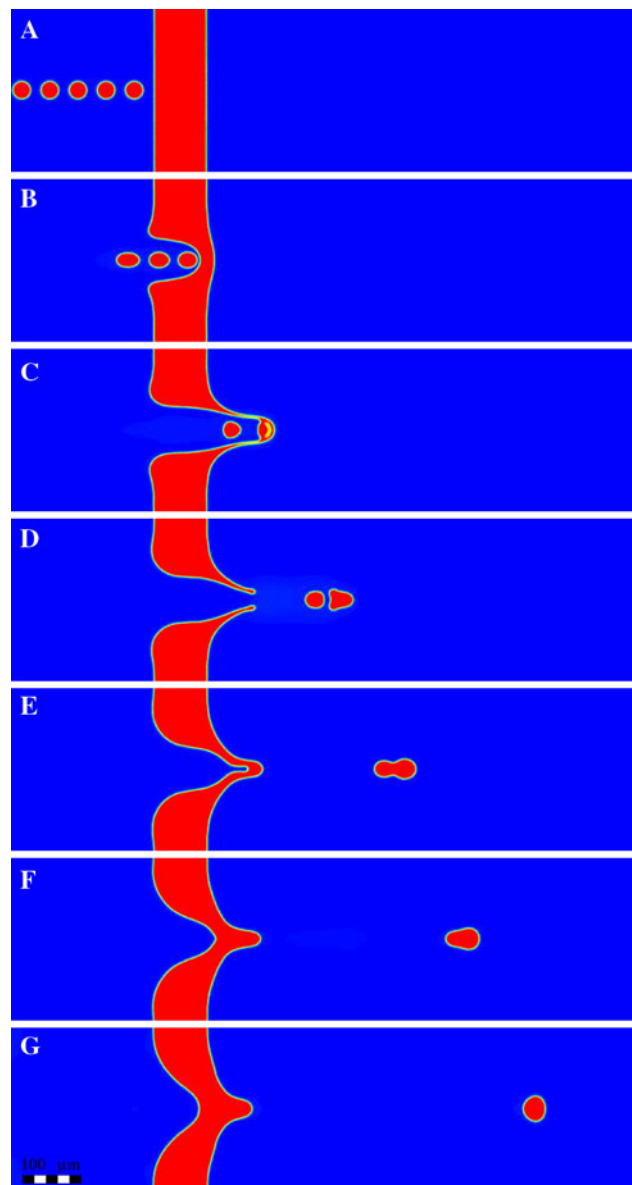


**Fig. 10** A sequence of pictures of five droplets impact and penetrate the liquid thin film. The initial speed  $u_1 = 13.2 \text{ m s}^{-1}$ ; **a**  $t = 0 \mu\text{s}$ , **b**  $15.2 \mu\text{s}$ , **c**  $30.4 \mu\text{s}$ , **d**  $45.6 \mu\text{s}$ , **e**  $60.8 \mu\text{s}$ , **f**  $76 \mu\text{s}$  and **g**  $91.2 \mu\text{s}$

$u_1 = 13.2 \text{ m s}^{-1}$ . In the right figure, the solution at  $t = 45.6 \mu\text{s}$  obviously shows that the droplet is completely trapped in the film, which reverts to the original form due to the surface tension force.

Note that, the droplet with diameter of  $2R = 54 \mu\text{m}$ , is the one we can compute from total volume of a drop ejected at the printhead, 80 pl. However, as observed in the experiments, in fact it did not form a single droplet, but a primary one with a long tail of satellites behind. Therefore, in next simulation, the effect of the different setup of the initialised droplets on the impact between them and the thin liquid film is examined. Figure 9b and c shows the impact between the liquid thin film with three droplets with diameter of  $2R = 37.4 \mu\text{m}$  and five droplets with diameter of  $2R = 31.6 \mu\text{m}$ , giving the same total volume in all three cases. The kinetic energy of the droplets in those three case is constant,  $E_k = 6.32 \times 10^{-9} \text{ pJ}$ . But the total surface energy for each initial case is different, which are  $E_s = 2.9 \times 10^{-10}$ ,  $4.2 \times 10^{-10}$  and  $5.0 \times 10^{-10} \text{ pJ}$  for Fig. 9a–c, respectively.

Evidently, the effect of the position and size of the initial dispenser droplets is strong. Figure 9b demonstrates that three smaller satellite droplets come closer to penetrating than in the case of one single bigger droplet (see Fig. 9a), but it is still not sufficient. The energy of droplets almost is lost. They are trapped in the thin liquid film, which went back to the original form after long simulation.

The introduction of five satellite droplets as shown in Fig. 9c not only increases the total energy of the system but also extends the impact time of droplets to the liquid thin film. Consequently, it gives more time for the thin film to develop and have a secondary droplet released from the thin film. The observation from numerical results are agree well with experiment.

**Fig. 11** Velocity profile after the droplets passed through the liquid thin film—the solution at  $t = 45.6 \mu\text{s}$

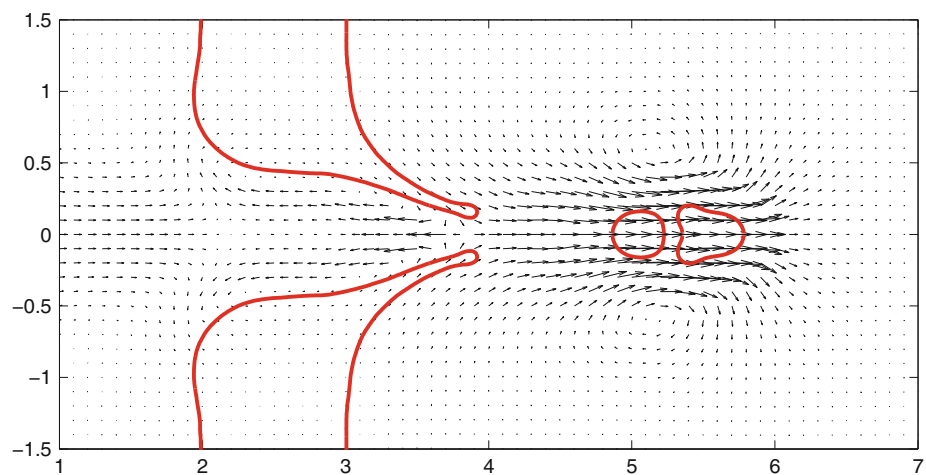
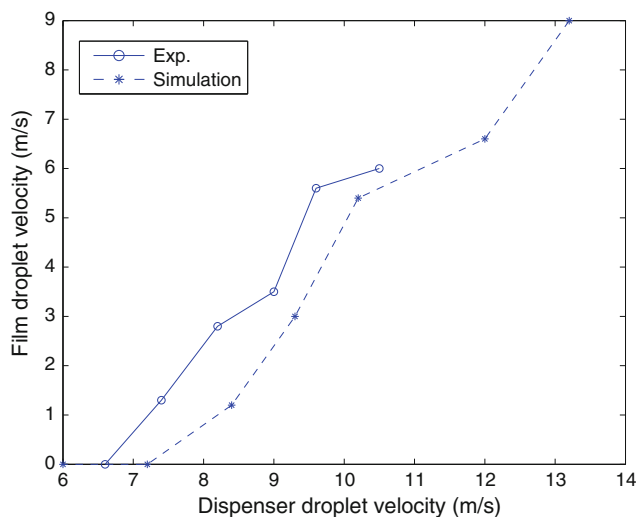


Figure 10 shows a sequence of pictures for the case shown in Fig. 9c. In Fig. 10b, the first two droplets have already touched the thin film. However, the energy of those two droplets is not sufficient to generate the second droplet behind the thin film until four droplets hit to the film as shown in Fig. 10c. The energy transferred to the thin film seems to be strong enough and the time is also long enough to generate the secondary droplet behind the thin film later as shown in Fig. 10d. It snaps the thin film and continues flying with its remaining momentum.

The whole sequence of Fig. 10 shows an agreement with the experiment in which the liquid thin film functioned as a filter for satellite droplets, Geyl et al. (2006). In this simulation, the initialisation droplets by a set of small droplets instead of a big one make the numerical picture more close to the experiment. Note that the leftmost droplet is elongated, even before it reaches the liquid film. This is no doubt caused by the rapid airflow created around the impact. A change in the volume of droplets occurred in the numerical simulation and 60 pl remained after shot 80 pl through the thin liquid film.

Figure 11 shows the velocity profile at  $t = 45.6 \mu\text{s}$ . When droplets pass through the thin liquid film, a vortex around the secondary droplet is formed and forces this film droplet to continue moving with the remaining velocity. Also there are several vortices around the thin film and those vortices force the thin film back to normal shape by surface tension force.

Recorded remaining speed,  $u_2$ , of droplets after passing through the thin film is found to strongly depend on the initial speed of droplets (dispensing velocity,  $u_1$ ), Fig. 12. As shown in this figure, the dependency of  $u_2$  on  $u_1$  is similar between numerical results and experimental results. In all the simulations shown in Fig. 12, the liquid



**Fig. 12** Plot of the residual velocity of droplets after it passed through the thin film versus the initial velocity

volume of the printhead was distributed in five equal droplets.

## 8 Conclusions

In this study, an experimental study and a numerical simulation of micro two-phase flows with high density difference has been carried out. A diffuse interface formulation, namely, the phase-field method, is employed to capture the interface. The numerical results indicate that this method can successfully simulate the impact, mixing and pinch-off when a droplet is shot at a thin liquid film.

A series of simulations are performed that match the experimental conditions. The numerical result helps to understand the importance of the surface energy of the microdroplets when they impact with a thin liquid film. It also gives a detailed view of the generation of the secondary droplet behind the thin liquid film.

It was found that a sequence of five smaller droplets could easily penetrate the film, where a single larger droplet would not. This may seem surprising, since the total liquid volume and the initial speed, and thus the total momentum of the impact, was the same in both cases.

However, when the volume is divided into a larger number of smaller droplets, the surface energy is partially converted to kinetic energy, and this helps the incident liquid to penetrate.

**Acknowledgment** This research is supported by VR (The Swedish Research Council) under the grant No: 2008-3950. Computer time provided by SNIC (Swedish National Infrastructure for computing) is gratefully acknowledged.

## References

- Amberg G, Töhnhardt R, Winkler C (1999) Finite element simulations using symbolic computing. *Math Comput Simulat* 49:149–165
- Barbulovic-Nad I, Lucente M, Sun Y, Zhang M, Wheeler A, Bussmann M (2006) Bio-microarray fabrication techniques—a review. *Crit Rev Biotechnol* 26(4):237
- Cahn JW, Hilliard JE (1958) Free energy of a nonuniform system. I. interfacial free energy. *J Chem Phys* 28(2):258–267
- Davis T (2004) Algorithm 832: UMFPACK, an unsymmetric-pattern multifrontal method. *ACM Trans Math Softw* 30(2):196–199
- Do-Quang M, Amberg G (2009) The splash of a solid sphere impacting on a liquid surface: numerical simulation of the influence of wetting. *Phys Fluids* 21:022102
- Do-Quang M, Villanueva W, Singer-Loginova I, Amberg G (2007) Parallel adaptive computation of some time-dependent materials-related microstructural problems. *Bull Pol Acad Sci* 55(2):229
- Ducrée J, Gruhler H, Hey N, Müller M, Békési S, Freygang M, Sandmaiser H, Zengerle R (2000) Topspot—a new method for the fabrication of microarrays. In: Proceedings of the 13th IEEE annual international conference on MEMS, Miyazaki, Japan, p 317
- Geyl A, Amberg G, van der Wijngaart W, Stemme G (2006) Study of the flight of small liquid droplets through a thin liquid film for picolitre liquid transfer. In: Proceedings of 19th IEEE international conference on MEMS, Istanbul
- Guermond JL, Quartapelle L (2000) A projection fem for variable density incompressible flows. *J Comput Phys* 165(1):167–188
- Jacqmin D (1999) Calculation of two-phase Navier-Stokes flows using phase-field modeling. *J Comput Phys* 155:96–127
- Jianping L, Guiling D (2004) Technology development and basic theory study of fluid dispensing—a review. In: Proceedings of the sixth IEEE CPMT conference on high density microsystem design and packaging and component failure analysis (HDP’04), Shanghai, China, p 198
- Le HP (1998) Progress and trends in ink-jet printing technology. *J Imaging Sci Technol* 42(1):49
- Villanueva W, Amberg G (2006) Some generic capillary-driven flows. *Int J Multiph Flow* 32:1072–1086